Air Separation by Integrally Asymmetric Hollow-Fiber Membranes

Xianshe Feng, John Ivory, and Varagur S. V. Rajan
Alberta Research Council, Edmonton, Alberta, Canada T6N 1E4

Integrally asymmetric hollow-fiber membranes each with an outer skin layer and a porous substrate were studied for air separation to produce nitrogen and oxygen enriched air. The test on both bore-side feed and shell-side feed with cocurrent and countercurrent flow arrangements for a wide range of stage cuts shows that the bore-side feed countercurrent flow was the most advantageous configuration in the permeator design. When operated in the bore-side feed countercurrent configuration, the permeator performance compared favorably with the commercial systems available for nitrogen production. A mathematical model was developed for this configuration. Since the concentration polarization in the substrate was a major concern for the bore-side feed configuration, especially for high stage-cut operations, a theoretical approach was pursued to formulate the concentration polarization. This allows for the diagnosis of the significance of concentration polarization in a specific permeation process, although it is difficult to predict concentration polarization accurately due to limited knowledge of the detailed membrane structure.

Introduction

Air separation for producing nitrogen and oxygen (or oxygen-enriched air) has been of great importance in the gas industry. Membrane air separation is now widely accepted as an economic process to produce moderate purity streams containing up to 99.5% nitrogen or 30–50% oxygen. It is estimated that air separation by membranes represents about 60% of the overall membrane gas separation business (Crull, 1998). Typical applications of the membrane-produced nitrogen include blanketing, purging, inerting, and underbalanced drilling, while the oxygen-enriched air is mainly used for combustion enhancement in furnaces and fuel cells, medical respiration, and undersea breathing. Membrane gas separation is based on the relative permeation rate of different components in a gas mixture through the membrane under the driving force of a pressure differential across the membrane.

For the present generation of membranes, the permeation selectivity to oxygen and nitrogen is relatively low; the permeability ratio is generally between 3 and 7. Consequently, the production of relatively pure oxygen would require multistage operations, each stage requiring recompression of the oxygen-enriched permeate stream from the previous stage. Currently, there are no membrane systems that produce high purity oxygen by the membrane process alone, while the membrane processes for the production of moderate purity nitrogen is practically viable. When high purity nitrogen is desired, hybrid separation processes that incorporate membranes with other "finishing" technologies [such as pressure swing adsorption (PSA), liquefaction, and deoxo process (Beaver et al., 1988; Schaub, 1991; Campbell et al., 1992; Prasad et al., 1994)] have been developed to eliminate the purity limitations of the membrane process while taking advantage of its efficient bulk separation characteristics.

In air separation by a membrane, air is fed to one side of the membrane, and nitrogen is obtained in the residue effluent at a pressure slightly lower than the feed pressure, whereas the permeate stream, maintained at a substantially lower pressure, is enriched with oxygen. The primary product stream is often targeted at either nitrogen or oxygen-enriched air due to purity and recovery considerations. In some cases where both product streams are required, a combination of membrane and PSA has been developed to en-

Correspondence concerning this article should be addressed to X. Feng at the following current address: Chemical Engineering Dept., University of Waterloo, Waterloo, Ontario, Canada N2L 3G1.

hance the overall separation efficiency (Lagree and Thompson, 1993). Despite the early interest in oxygen enrichment of air by membranes and the extensive economic evaluation of the processes (see, for example, Bhide and Stern, 1991a,b) oxygen enrichment by membrane is presently not as well developed as for nitrogen production, probably due to the relatively small market size and strong competition from PSA.

It is well known that besides the membrane permselectivity and operating pressures, the pattern of permeate flow with respect to feed flow (such as countercurrent, cocurrent, or cross flow) generally influences the separation performance of a membrane permeator. The flow pattern is an important consideration in the design of industrial membrane separators. At a given stage-cut, which is defined as fractional feed permeated through the membrane, the countercurrent flow normally gives a better separation. However, it was shown that in the case of high flux asymmetric membranes that comprise a permselective skin layer and a porous support layer, when the skin layer faces with the feed gas, the permeate-feed flow pattern has little effect on the separation performance and the permeator always exhibits the cross-flow type of permeation behavior because the high permeate velocity through the porous substrate prevents the mixing of local permeate fluxes (Pan, 1983, 1986). In such cases, the countercurrent flow pattern is not necessarily the preferred operating mode. This was found to be true for the separations of H_2/N_2, He/CH_4 and CO_2/CH_4 gas mixtures by hollow fiber membranes where the membrane permeance to the "fast" gas was of the order of 10^{-4} $cm^3(STP)/(cm^2 \cdot s \cdot cmHg)$. For air separation, the oxygen permeability is about one order of magnitude lower, and the operating pressure, normally ranging from 70 to 190 psig (0.48 to 1.31 MPa gauge), is relatively low. It has not been clarified whether the permeation flux in air separation is high enough to overcome the effects of local permeate mixing due to back diffusion in the porous substrate of the membrane. When the permeate flux is sufficiently low, the local permeate mixing will become significant and the flow pattern is expected to impact the permeator performance.

Gas separation membranes in the form of asymmetric and/or composite hollow fibers are widely used mainly due to their high packing density and self-supporting characteristics. The hollow fibers are normally arranged in a shell-and-tube configuration. In principle, the feed gas may be supplied to either the shell side or the bore side of the hollow fiber permeator. In the shell-side feed configuration, the feed gas enters the permeator on the shell side and the permeate is collected from the fiber bores. In the simplest version, only one active tubesheet is needed to allow for permeate removal from the fiber lumens. This design is simple and the module assembling is straightforward, but provisions must be made to pack the fibers uniformly in order to achieve a uniform flow distribution. In the bore-side feed configuration, on the other hand, the feed gas enters the fiber bores at one end of the hollow fibers, and the residue exits from the fiber lumens at the other end, whereas the permeate is removed from the shell side of the device. This requires two active tubesheets, one at each end of the hollow fibers. In the latter configuration, a more even flow distribution of feed on the membrane surface is achieved, which is beneficial to an efficient operation. Also, only the fiber wall and the end caps of the membrane device are pressurized, and the pressure at the shell side is substantially low. Therefore, the mechanical strength requirement to the shell casing of the permeator is minimized. However, when the pressurized gas stream moves to or from the fiber bores, both tubesheets are under significant compressive and sheer stresses. Consequently, the bore-side feed permeator design is more complicated than the shell-side feed design because of the problems associated with supporting the tubesheets (Caskey et al., 1990a,b; Etienne et al., 1995; Kalthod, 1996). Obviously, the choice of bore-side or shell-side feed should be determined by the cost of manufacturing and the separation performance of the permeator; both modes of feed are being used presently in commercial hollow fiber membrane permeators for nitrogen production. It should be mentioned that the prior work on hollow fiber membrane modules is mainly directed at the shell-side feed configuration, and systematic studies of the bore-side feed configuration are lacking. This is presumably due to the fact that the shell-side feed configuration was primarily used in the early commercial hollow fiber membrane modules.

One of the objectives of this work was to test the performance of air separation using the integrally asymmetric hollow fiber membranes that were originally developed by the Alberta Research Council (ARC) for helium and hydrogen recovery on industrial scales. A small-scale hollow fiber permeator was constructed and tested over a wide range of stage-cut for different flow patterns and module configurations that are of interest to the engineering design of permeators. The bore-side feed countercurrent flow was shown to be the most efficient configuration of permeator design in the present study, and a mathematical model was developed for this configuration. However, a potential concern with this configuration was the concentration polarization in the porous substrate of the membranes, and the significance of the concentration polarization was analyzed with case studies for membrane air separation.

Experimental Studies

A bundle of 368 hollow fibers were encased in a 3/8-in. (9.5-mm) OD copper tubing and arranged in a shell-and-tube configuration. The hollow fibers had an integrally asymmetric structure with an outer dense skin layer supported on a porous substrate. Both ends of the fiber bundle were potted with an epoxy resin to form fluid-tight tubesheets, and the tubesheets were serviced to make the fiber bores open. The active fiber length was 25 cm, and the length of the fibers embedded in each tubesheet was 2.8 cm. The effective membrane area for permeation was 462 cm^2 based on a nominal fiber outside diameter of 160 μm. The module was constructed such that the feed air can be introduced to either the bore side or the shell side of the device in either countercurrent or cocurrent feed-permeate flow patterns. Special caution was exercised in the module construction to ensure that all the fiber bores at both ends of the membrane module were fully open. The membrane module is illustrated in Figure 1, which also shows the experimental setup for the shell-side feed countercurrent flow arrangement. The setup was slightly modified by changing the gas inlet and outlet appropriately to suit other flow and feeding arrangements.

The pure gas permeation experiments were carried out in the same setup with the residue outlet port being closed to

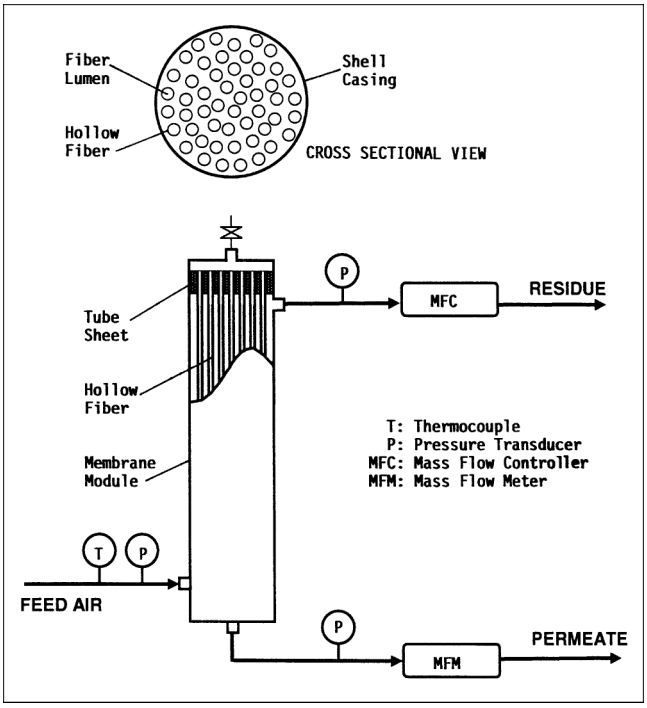

Figure 1. Membrane module and the experimental setup.

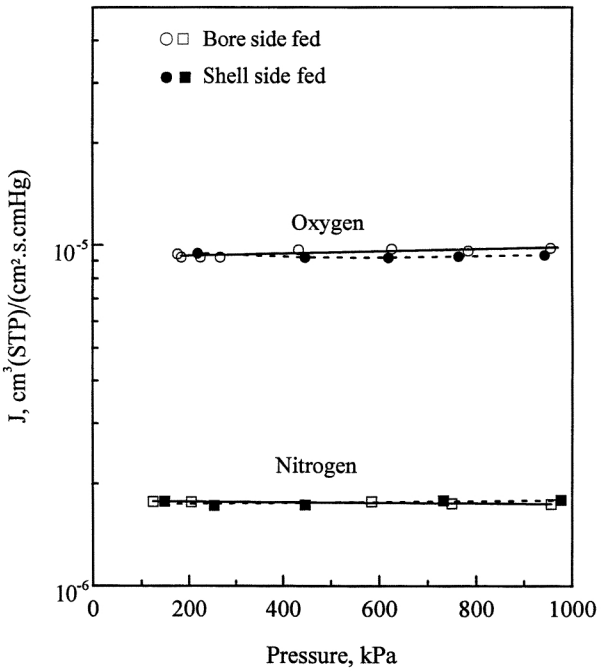

Figure 2. Permeance of the hollow fiber membrane to oxygen and nitrogen at 23°C.

1 $cm^3(STP)/(cm^2 \cdot s \cdot cm\ Hg) = 3.35 \times 10^{-4}$ $mol/(m^2 \cdot s \cdot Pa)$.

determine the individual permeabilities of oxygen and nitrogen. In air separation tests, cylinder air containing 20.5 vol. % O_2 (balance N_2), supplied by Praxair Inc., was used as the feed gas. The feed gas was admitted to the membrane module at a predetermined pressure, and the flow rate of the residue stream exiting the membrane module was controlled by a Matheson mass-flow controller. The flow rate of the permeate stream was measured by a mass-flow meter. Unless specified otherwise, the permeate stream exited the membrane device at atmospheric pressure. When the permeate side was to be maintained at a subatmospheric pressure, a diaphragm vacuum pump was employed. Most of the tests were conducted under isothermal conditions at the ambient temperature (23°C), and a thermal bath was used for other operating temperatures. The compositions of all the gas streams (feed, permeate, and residue) were analyzed using a Varian gas chromatograph equipped with a thermal conductivity detector. The experiments covered a wide range of stage-cuts; a relatively low stage-cut was used for producing oxygen enriched air, and the production of nitrogen would require a high stage-cut operation.

Results and Discussion

Membrane permeability

The measured permeance of pure oxygen and nitrogen at different pressures through the hollow fiber membranes is shown in Figure 2. It is shown that the nitrogen permeability is essentially constant over the pressure range tested irrespective of shell-side feed or bore-side feed, while the oxygen permeability in the bore-side feed mode is only slightly higher ($< 3\%$) than in the shell-side feed. This suggests that the effects of mechanical stress applied to the hollow fibers due to the pressure differential across the fiber wall is insignificant, at least in the pressure range tested. Thus, the permeability of the gas component in a gas mixture can be assumed to be the same as the pure gas permeability.

Figure 3 shows the effect of temperature on the membrane permeance, which follows the Arrhenius type relationship as expected. The activation energy for the permeation of oxygen and nitrogen is calculated to be 19.3 and 27.6 kJ/mol, respec-

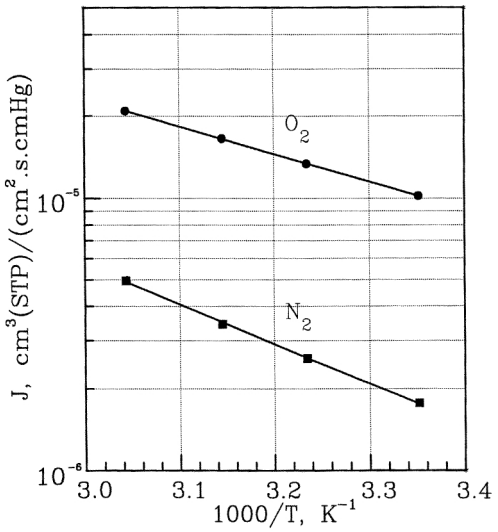

Figure 3. Effect of temperature on membrane permeance.

1 $cm^3(STP)/(cm^2 \cdot s \cdot cm\ Hg) = 3.35 \times 10^{-4}$ $mol/(m^2 \cdot s \cdot Pa)$.

tively. An increase in temperature enhances the membrane permeability, while the selectivity, which can be characterized by the permeability ratio of oxygen to nitrogen, decreases. This implies that at a given stage-cut, increasing the operating temperature will increase the productivity of the membrane system, but at the expense of reduced product purity. It can be seen from Figure 3 that in the typical operating temperature range of 1–45°C, for every 10°C increase in the temperature, the oxygen permeability will increase by 25–35%, whereas the oxygen/nitrogen selectivity will decrease by about 10%. Consequently, for the practical situation of designing a membrane system to deliver a certain amount of purified product at a given purity, the temperature effect is somewhat self-compensating. The optimal operating temperature should be determined by the overall considerations of the membrane characteristics and the cost of after-compressor cooling.

Air separation

Effects of Flow Configurations. The concentrations of nitrogen in the residue stream and oxygen in the permeate stream are plotted in Figures 4 and 5, respectively, as a function of stage-cut for the following four flow configurations:

(1) Bore-side feed countercurrent flow
(2) Bore-side feed cocurrent flow
(3) Shell-side feed countercurrent flow
(4) Shell-side feed cocurrent flow

As mentioned earlier, if the permeation flux is very high, the radial mixing of local permeate will be negligible, and the membrane performance will follow the cross-flow behavior, irrespective of countercurrent or cocurrent flow (Pan, 1983, 1986). It is apparent from the results in Figures 4 and 5 that this is not the case for the air separation studied here, and the countercurrent feed/permeate flow pattern is shown to be advantageous over the cocurrent flow pattern. Further, it is also shown that the bore-side feed gives a better separation than the shell-side feed, though the difference is insignificant for producing relatively high purity ($>98\%$) nitrogen at a high stage cut.

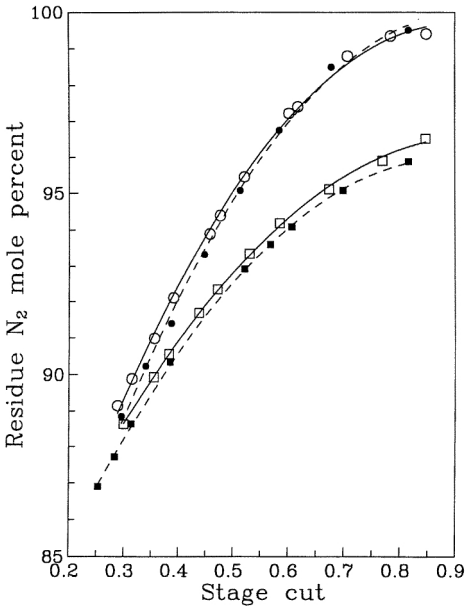

Figure 4. Nitrogen concentration in residue stream as a function of stage-cut.

Feed pressure 100 psig (690 kPa) and permeate pressure 0 psig. Temperature 23°C. (○) bore-side feed countercurrent flow; (●) shell-side feed countercurrent flow; (□) bore-side feed cocurrent flow; (■) shell-side feed cocurrent flow.

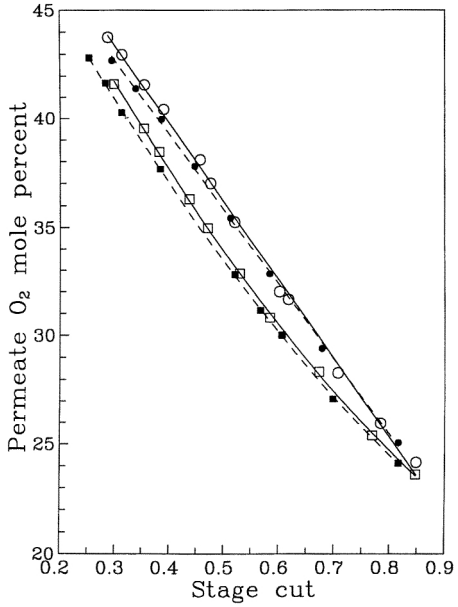

Figure 5. Oxygen concentration in permeate stream as a function of stage-cut.

Test conditions were the same as those given in Figure 4.

In assessing the performance of a membrane permeator, three issues need to be addressed: product purity, recovery, and productivity. Here, the product recovery is defined as the fraction of nitrogen or oxygen in air recovered as product, and the productivity is defined as the amount of product in terms of equivalent pure nitrogen or oxygen generated per unit time per unit membrane area. For all the four flow configurations studied, the productivities of nitrogen in the residue and oxygen in the permeate as a function of product purity are shown in Figures 6 and 7, respectively. While the productivity of nitrogen decreases with an increase in its purity, the opposite is true for oxygen enrichment. For both oxygen enrichment and nitrogen production, increasing product purity always reduces the product recovery, and the reduction in the recovery becomes more profound at higher product purities, as shown in Figures 8 and 9. This means that there is a trade-off relationship between product recovery and purity; either a high recovery or a high purity can be obtained in the membrane processes, but seldom both. For a required purity, a higher recovery rate means lower specific energy consumption, which is often the major operating cost. Therefore, for a given membrane system, the operating conditions should be optimized in order for the separation potential of the membrane to be maximized.

The above results demonstrate that the permeator in the bore-side feed countercurrent flow configuration performs the best. This flow configuration was used in all subsequent tests.

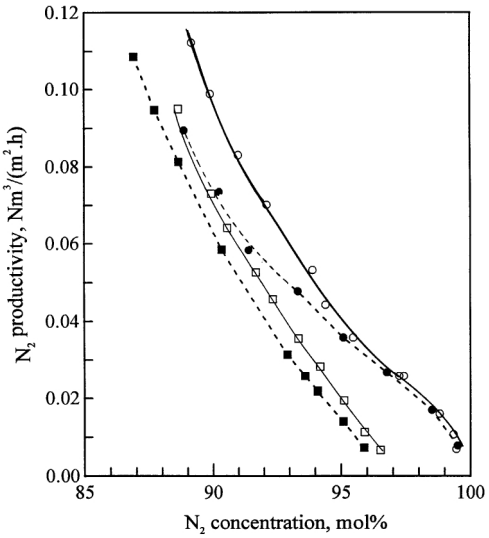

Figure 6. Productivity of nitrogen vs. concentration of the nitrogen stream.

Test conditions were the same as those given in Figure 4.

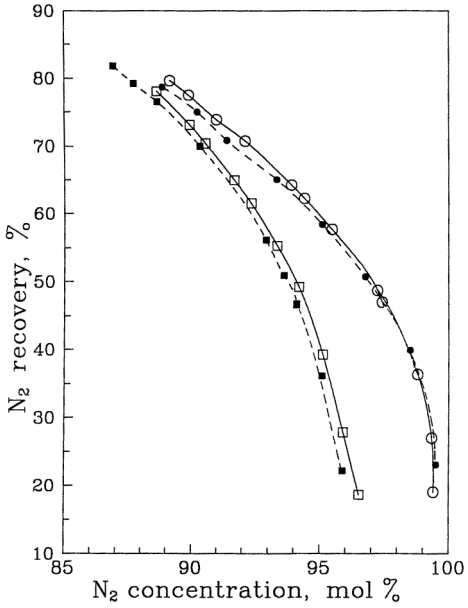

Figure 8. Trade-off relationship between recovery and concentration for nitrogen production.

Test conditions were the same as those given in Figure 4.

While the countercurrent flow is normally the preferred configuration, both bore-side feed and shell-side feed have been used in commercial membrane systems, especially for nitrogen production. The purity level of membrane-produced nitrogen is practically in the range of 95–99.5%. Figure 10 shows the relative nitrogen productivity at different nitrogen purity levels as compared to some commercial systems including Balston (1997), Prism (1995), NitroGEN (1993) and UBE (1997), taking the nitrogen productivity at 95% purity as 1. Clearly, the hollow fiber membranes used in the present study compares favorably with the commercial units. In general, the productivity decreases as product purity increases. As a rule of thumb, the productivity is halved when the nitrogen purity changes from 95 to 98%.

It may be mentioned that in the bore-side feed mode, the fiber lumen is pressurized, and the dense skin layer, which is on the outer surface of the hollow fiber, is no longer supported mechanically by the porous substrate. For air separation where a moderate operating pressure is usually used, the mechanical strength of the currently available membranes is generally sufficient to bear the stress applied to the fibers regardless of whether the feed is applied to the bore side or the shell side. In the bore-side feed, however, stagnant gas zones are likely to be present in the porous substrate of the hollow fibers as the feed gas passes down the fiber lumen. Due to retention of the slow permeating component by the

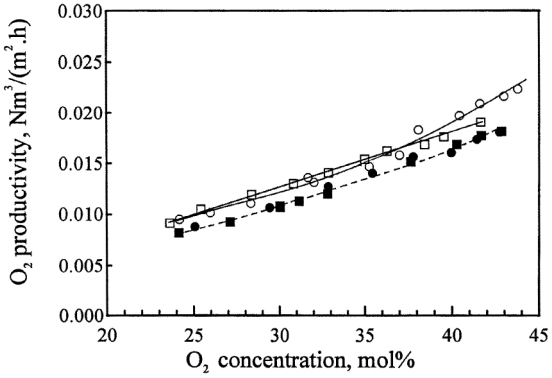

Figure 7. Productivity of oxygen vs. concentration oxygen-enriched air stream.

Test conditions were the same as those given in Figure 4.

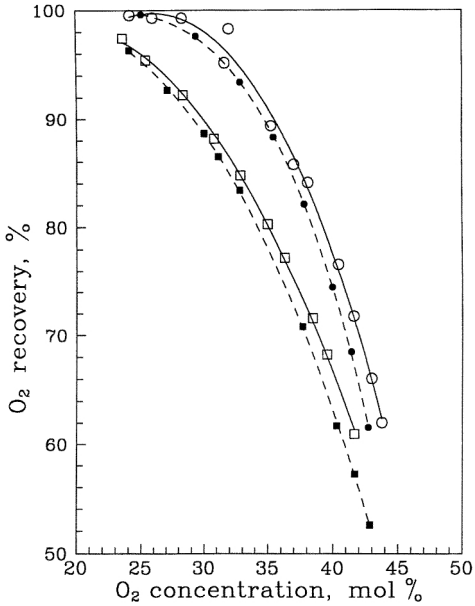

Figure 9. Trade-off relationship between recovery and concentration for oxygen enrichment of air.

Test conditions were the same as those given in Figure 4.

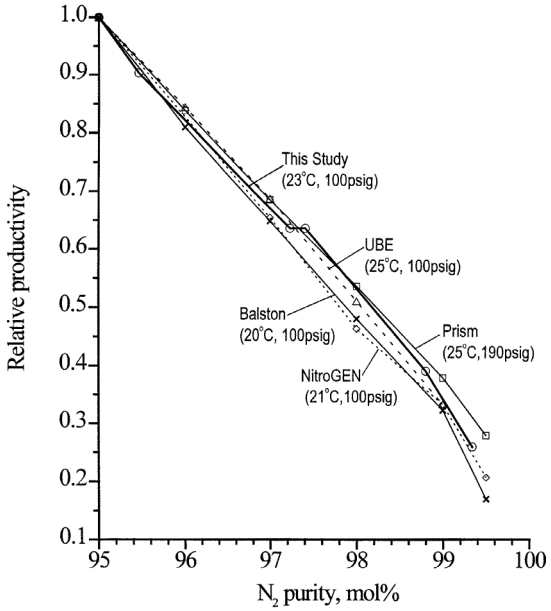

Figure 10. Membrane used in this study vs. commercial membrane systems for nitrogen production.

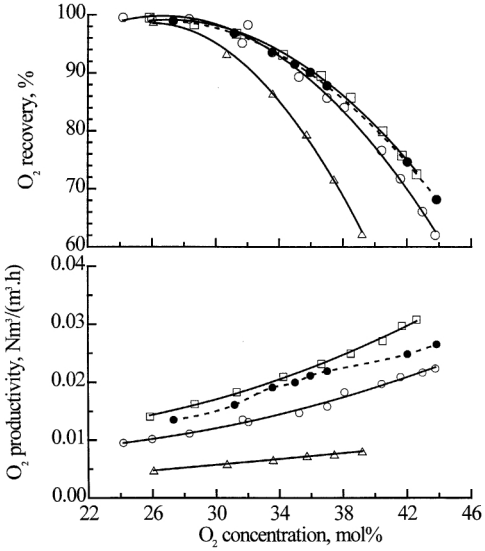

Figure 12. Effect of operating pressure on the permeator performance for oxygen enrichment.

Testing conditions were the same as those given in Figure 11.

membrane, a concentration gradient is built up in the stagnant gas zones in the substrate. This is referred to as concentration polarization. Therefore, concentration polarization in the membrane substrate is an obvious concern. If such an effect is significant, the separation performance of the permeator will be deteriorated. The significance of concentration polarization is further discussed in more depth later.

Effects of Operating Pressure and Temperature. Figures 11 and 12 show the productivity and recovery of nitrogen in the residue and oxygen in the permeate respectively at different operating pressures as a function of product purity. A feed pressure of 100 psig (690 kPa) and atmospheric pressure of permeate (local value of 70 cmHg absolute) were used as the base case. It is interesting to note that increasing the feed pressure by 50 psi (345 kPa) from the base case condition is essentially equivalent to evacuating the permeate at 57 cmHg vacuum for the production of 95% + nitrogen. Similar results are also true for oxygen enrichment except that the oxygen productivity with the permeate evacuation operation is approximately 13–17% lower than the productivity with the elevated feed pressure. As expected, for a given product purity, increasing the feed pressure and/or decreasing the permeate pressure will increase the product recovery and productivity. In other words, an increase in feed pressure and a decrease in permeate pressure will reduce the membrane area required for a given separation task because of the increased driving force for permeation. In principle, the driving force for permeation can be provided by pressurizing the feed, evacuating the permeate, or a combination of both. The overall economics of capital costs of the compressor and/or vacuum pump, as well as the operating costs, should be taken into account in determining the optimal operating pressure. Evacuation of the permeate stream is occasionally used for oxygen enrichment using low-selectivity silicone rubber based membranes, and the vacuum system is an important part of the overall costs of the process (Bhide and Stern, 1991b). Compressed air is typically used as feed for nitrogen production with permeate being discharged at essentially atmospheric pressure.

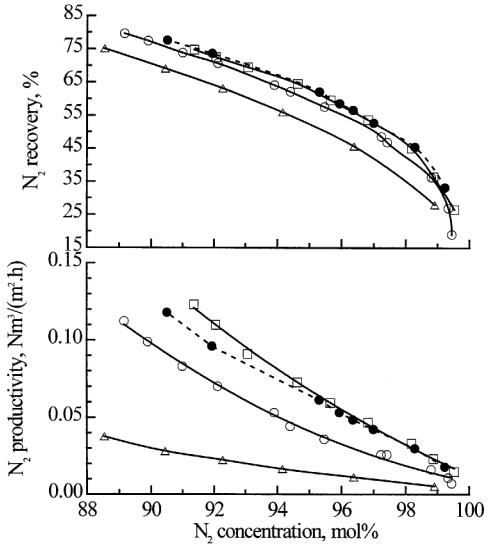

Figure 11. Effect of operating pressure on the permeator performance for nitrogen production.

Temperature 23°C. Feed pressure (□) 150 psig; (○, ●) 100 psig; (△) 50 psig; permeate pressure 0 psig except for (●) for which 57 cm Hg vacuum was applied.

The effects of operating temperature on the separation performance are presented in Figures 13 and 14. As mentioned earlier, as the temperature increases, the membrane permeability increases and the permeation selectivity decreases. The experimental data in the figures, represented by the symbols, show that, for production of 95% nitrogen, an increase in the temperature from 23 to 45°C will increase the

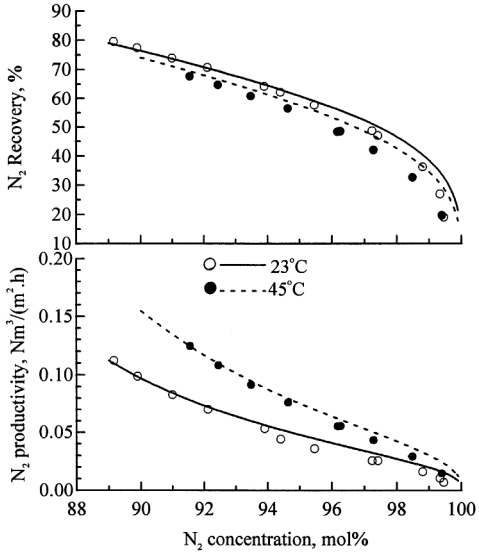

Figure 13. Effect of operating temperature on the permeator performance for nitrogen production.

Feed pressure 100 psig (690 kPa) and permeate pressure 0 psig. Temperature (○) 23°C; (●) 45°C. Lines in the figure represent the model predicted data assuming negligible concentration polarization.

nitrogen productivity by about 75%, which is accompanied by a loss in recovery of about 8%. For the production of 35% oxygen, the same temperature change will double the productivity, with approximately 6% loss in recovery. For air separation, the "raw" material (that is, feed air) is "free" and only the operating costs are primarily affected by the product recovery. It thus appears that the beneficial effects of increasing the temperature for increased productivity outweigh the detrimental effects of reduced recovery. However, the maximum operating temperature is often restricted by the thermal properties of the membranes.

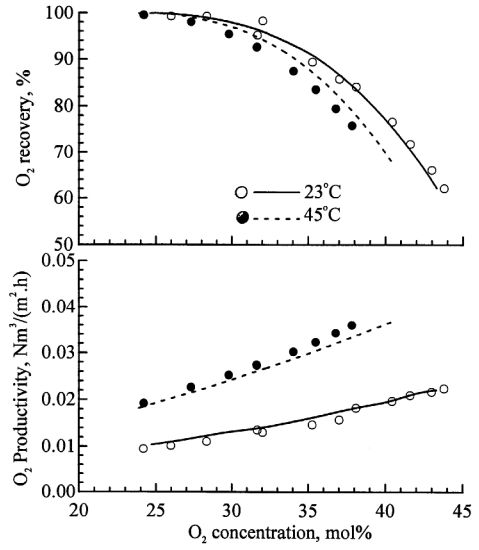

Figure 14. Effect of operating temperature on the permeator performance for oxygen enrichment.

Test conditions were the same as those given in Figure 13. Lines in the figure represent the model predicted data assuming negligible concentration polarization.

Modeling of hollow fiber permeators with bore-side feed countercurrent flow

Although there are numerous models reported in the literature on hollow fiber permeators, most of them are directed at shell-side feed operations. As shown earlier, the bore-side feed countercurrent flow arrangement is the best configuration for air separation using asymmetric hollow fiber membranes. A mathematical model is thus developed here for this configuration.

The key assumptions made in the model development are: (1) the deformation of the hollow fiber under pressure is negligible; (2) the membrane permeability is independent of concentration and pressure; (3) the pressure change of permeate stream in the shell side is negligible; and (4) the gas flow in the fiber lumen follows the differential form of the Hagen-Poiseuille equation for laminar flow. For simplicity, consider the permeation of a binary gas mixture. Figure 15 illustrates the permeation through an asymmetric hollow fiber membrane. If the concentration polarization on the feed side (fiber lumen) is negligible, the following relationships can be formulated

Permeation

$$\frac{d(UX)}{dZ} = N\pi d_o J_1(PX - pY) \tag{1}$$

$$\frac{d[U(1-X)]}{dZ} = N\pi d_o J_2[P(1-X) - p(1-Y)] \tag{2}$$

Mass balance

$$U = U_0 + V \tag{3}$$

$$UX = U_0 X_0 + VY \tag{4}$$

Pressure drop in the fiber lumen

$$\frac{dP}{dZ} = \frac{128RT\mu}{N\pi d_i^4 P}U \tag{5}$$

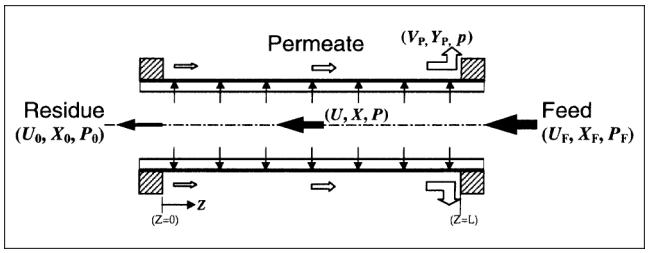

Figure 15. Asymmetric hollow-fiber membrane operating in bore-side feed countercurrent flow configuration.

Adding Eqs. 1 and 2 gives

$$\frac{dU}{dZ} = N\pi d_o J_1\{(PX - pY) + [P(1-X) - p(1-Y)]/\alpha\} \tag{6}$$

where $\alpha = J_1/J_2$, which is the separation factor expressed in terms of the permeance ratio.

Rearranging Eq. 1 gives

$$\frac{dX}{dZ} = \frac{1}{U}\left[N\pi d_o J_1(PX - pY) - X\frac{dU}{dZ}\right] \tag{7}$$

Combining Eqs. 3 and 4 yields

$$Y = \frac{UX - U_0X_0}{U - U_0} \tag{8}$$

Equations 5–8 constitute the basic equations describing the permeator behavior. They can be solved numerically over the active fiber length from the residue outlet ($Z = 0$), where the corresponding local permeate concentration Y can be obtained by solving

$$\frac{Y}{1-Y} = \frac{\alpha(PX - pY)}{P(1-X) - p(1-Y)} \tag{9}$$

which is based on cross-flow permeation. Note that the proceeding equations are similar to those for the shell-side feed permeators except that the gas pressure on the feed side changes along the fiber length.

For the inactive portions of the hollow fiber embedded in the tubesheets, the molar gas-flow rate U and composition X do not change, and the pressure change can be calculated from Eq. 5. For the practical problem of calculating membrane performance with specified product and feed concentrations, the computation can be converted into an initial value problem. Basically, to guess a value of residue flow rate U_0 at $Z = 0$, integrate Eqs. 5–7 (such as by Runge Kutta method) from $Z = 0$ to $Z = L$. Repeat the integration until the calculated concentration X_L matches the concentration of the feed X_F. This procedure is especially straightforward when the residue is the desired product (such as production of nitrogen from air) whose purity X_0 is a known quantity. When the permeate is the desired product, Y_P is known, and the computation procedure may be modified slightly by:

(1) Assuming a state-cut θ so that X_0 can be calculated from $X_0 = (X_F - \theta Y_P)/(1-\theta)$

(2) Guessing U_0 and performing the aforementioned procedure until calculated X_L agrees with X_F

(3) Adjusting the value of θ and repeating step 2 until the calculated permeate product concentration Y_P is satisfied.

The typical calculation results are illustrated in Figures 13 and 14 as compared to the experimental data. The model predicts the module performance quite well, but it seems that at high stage-cut operations for producing relatively high purity nitrogen, the model predictions are slightly overestimated. It is natural to suspect that the deviations are attributed to the concentration polarization, which was not taken into account in the calculations. In the shell-side feed permeation, when the permeation flux is sufficiently high, the local concentration of permeate in the porous substrate of the membrane differs from that of bulk permeate stream outside the substrate layer because of the lack of local permeate mixing. The same rationale also applies for the bore-side feed where the porous substrate is in contact with the feed; the presence of porous substrate renders the feed concentration that the membrane "sees" different from that in the bulk phase. It is of interest to determine whether the concentration polarization is significant.

Concentration polarization

Figure 16 is a simplified drawing of the membrane structure with an outer dense skin layer and a porous substrate. The permeation properties are primarily determined by the skin layer and a transition layer (with an inside radius r_2 (m)) between the substrate and the skin. The resistance of mass transfer in the transition layer by Knudsen diffusion through the fine pores is accounted for in the measured permeability of the membrane. For the present generation of membranes and under normal operating conditions, it can be estimated that the boundary layer mass-transfer coefficient for a laminar flow through the fiber lumen is high enough that the concentration polarization is unlikely to occur outside the porous substrate. Assume the concentration polarization takes place in a hollow cylindrical region in the substrate with an inside radius of r_1 and an outside radius of r_2. The value of r_1 can be as small as the radius of the fiber lumen, depending on the specific hydrodynamic conditions of the gas flow. It is further assumed that: (1) the pores in the substrate have a uniform size and distribution; (2) the pore size in the substrate is big enough to allow for gas transport by molecular diffusion; (3) the pores are open (complete penetration of pores through the substrate); and (4) the pores may be tortuous, but, at steady state, the total radial mass-transfer rate through a cylindrical plane of radius r relative to the axis of the fiber lumen is constant.

At steady state, the permeation flux through the membrane is equal to the net flux through the concentration polarization layer by diffusive and convective flows. For the permeation of a binary mixture, the following mass-transfer equations can be developed on the basis of "film theory" for

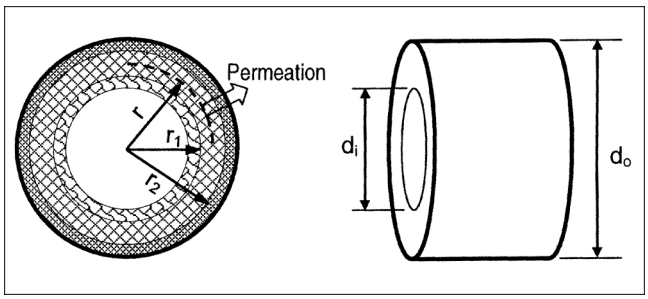

Figure 16. Asymmetric hollow-fiber membrane with an outer skin layer supported on a porous substrate.

a short fiber length l (m)

$$Q_1 = -2\pi rl\epsilon\left(\frac{D}{\tau}\right)C\frac{dX}{dr} + (Q_1 + Q_2)X \tag{10}$$

$$Q_2 = 2\pi rl\epsilon\left(\frac{D}{\tau}\right)C\frac{dX}{dr} + (Q_1 + Q_2)(1 - X) \tag{11}$$

where Q_1 and Q_2 are the molar permeation rates of the fast and the slow components through a hollow fiber with a length of l, respectively. X is the molar fraction of the fast component. ϵ and τ are the area porosity and tortuosity of the pores in the substrate (fraction), respectively. D is the gas-phase diffusion coefficient (m^2/s), and C is the total molar concentration (mol/m^3), which is equal to (RT/P) based on the ideal gas flow. Subject to the following boundary conditions

$$X = X_B \quad \text{at} \quad r = r_1$$
$$X = X_S \quad \text{at} \quad r = r_2$$

the above equations can be integrated to give

$$Q = \frac{2\pi l\epsilon C}{\ln(r_2/r_1)}\left(\frac{D}{\tau}\right)\ln\left(\frac{Y' - X_S}{Y' - X_B}\right) \tag{12}$$

where $Q = (Q_1 + Q_2)$ is the total molar permeation rate, and X_B and X_S are the concentrations in the bulk feed and on the membrane surface due to concentration polarization, respectively. Y' is a quantity equivalent to the local concentration of permeate leaving the membrane skin layer by cross-flow permeation and is given by

$$Y' = \frac{Q_1}{Q_1 + Q_2} \tag{13}$$

Define the molar average velocity ν and the mass-transfer coefficient k in a conventional manner

$$\upsilon = \frac{Q}{2\pi lr_m\epsilon C} \tag{14}$$

$$k = \frac{D}{\tau\delta} \tag{15}$$

where r_m is the log mean radius (m) of r_1 and r_2, and the linear mean can be used in practice where $(r_2/r_1) < 2$. δ $(= r_2 - r_1)$ is the thickness of the concentration polarization layer. Then, Eq. 12 can be rewritten as

$$\frac{Y' - X_S}{Y' - X_B} = \exp(\upsilon/k) \tag{16}$$

This is the fundamental equation describing concentration polarization. It suggests that concentration polarization is determined by the relative value of ν and k, which are dependent on the fluid hydrodynamic conditions, the structure of the porous substrate, and the permeability of the membrane. Obviously, X_S is always smaller than X_B for finite values of k. Only when k is substantially larger than υ will X_S approach X_B, in which case the concentration polarization is insignificant. The ratio X_S/X_B can be used to characterize the severity of concentration polarization. Similar relationships have been derived for pervaporation (Feng and Huang, 1994) and other membrane processes for liquid separations (Field, 1996).

To account for the effect of concentration polarization in the calculations, the quantity X in the foregoing permeator modeling equations should be substituted with X_S, which is related to the bulk gas concentration by Eq. 16. A detailed analysis of concentration polarization will require the knowledge of the pore structure of the membrane, which is often not readily available for the pores in the membranes are not straight and cylindrical but are irregular. As such, accurate predictions of the significance of concentration polarization are usually difficult, but Eq. 16 can be used to diagnose whether concentration polarization is significant in a specific process.

As an illustration, let us consider the "base case" permeation. Due to permeation, the velocity of gas flow in the fiber lumen decreases as the gas passes down the fiber bore, and the effect of concentration polarization, if present, tends to be most significant near the residue exit. As a first approximation, assume that the local mass-transfer coefficient k changes along the fiber length in a fashion similar to mass transfer for laminar flow inside a pipe by the Levêque equation, that is, k is proportional to the gas-flow velocity to the power of 1/3. Figures 17 and 18 show the calculated results that take into account the effect of concentration polarization for the base case permeation under an assumption of $X_S/S_B = 0.92$ (arbitrary) at $Z = 0$ for producing 98.5% nitrogen in the residue stream. The calculated results without ac-

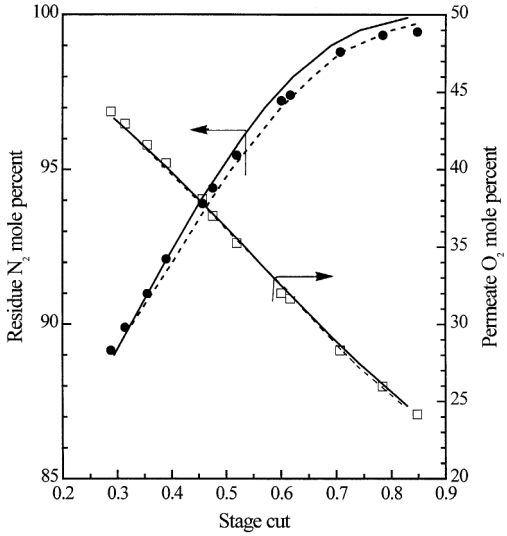

Figure 17. Calculated concentrations of permeate and residue as compared to experimental data for the "base case" permeation.

The dashed and solid lines represent respectively the calculated data with and without taking into account the concentration polarization.

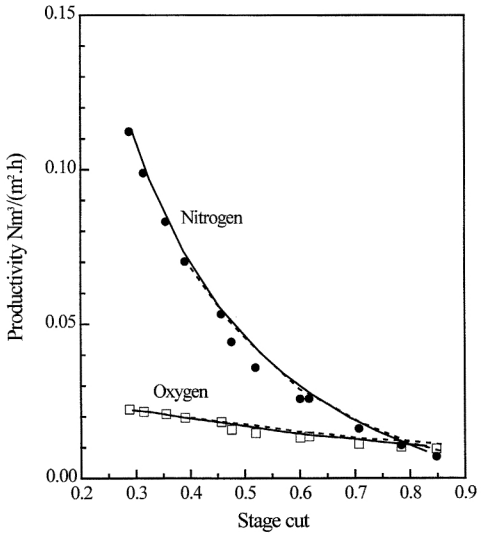

Figure 18. Calculated productivity of nitrogen in residue and oxygen in permeate as compared to experimental data for the "base case" permeation.

The dashed and solid lines represent respectively the calculated data with and without taking into account the concentration polarization.

counting for concentration polarization and the experimental data are also presented in the figures for comparison. It is shown that concentration polarization influences the product purity for nitrogen production at a high stage-cut more significantly than for oxygen enrichment at a low stage-cut, and in general the productivity is not considerably different from that predicted assuming no concentration polarization. This is understandable because concentration polarization tends to retard the permeation of fast gas and enhance the permeation of slow gas, rendering the residue concentration relatively more sensitive to concentration polarization than the productivity. A comparison of experimental data with the calculated results indicates that the significance of concentration polarization is at such a level of the concentration X_S that the membrane "sees" is greater than 92% of the bulk concentration for the air separation system studied here, which corresponds to a value of υ/k of greater than 0.95. It is estimated that the residue stream exited the fiber lumen at a linear velocity of the order of 1 cm/s. The concentration polarization is expected to pose more severe problems with highly permselective membranes under the same hydrodynamic conditions.

Conclusions

Integrally asymmetric hollow fiber membranes with an outer skin layer supported on porous substrate were investigated for air separation with case studies for the production of nitrogen and oxygen enriched air. Both bore-side feed and shell-side feed were tested experimentally with cocurrent and countercurrent flow arrangements for a wide range of stage-cuts, and the bore-side feed countercurrent flow was shown to be the preferred configuration of the permeator design especially for high stage-cut operations. When operated in the latter configuration, the membrane performance compared favorably with the commercial membrane systems for producing over 95% nitrogen. A mathematical model was developed for this configuration, and the separation performance was well predicted. The effects of operating pressure and temperature on the separation performance were evaluated. For shell-side feed, the permeator did not give rise to cross-flow type permeation in spite of the presence of the porous substrate, and for bore-side feed, the concentration polarization in the substrate was likely to occur. Starting from basic mass-transfer considerations, the concentration polarization was analyzed using a cohesive approach as those used in pervaporation and other membrane processes for liquid separation. Though accurate predictions of concentration polarization are difficult primarily due to limited knowledge of the detailed porous structure of the substrate, it has been demonstrated that the significance of concentration polarization can be diagnosed.

Notation

d_i = inside diameter of hollow fiber membrane, m
d_o = outside diameter of hollow fiber membrane, m
k = mass-transfer coefficient in concentration polarization layer, m/s
J = permeance, $cm^3(STP)/(cm^2 \cdot s \cdot cm\ Hg)$ [1 $cm^3(STP)/(cm^2 \cdot s \cdot cm\ Hg) = 3.348 \times 10^{-4}$ $mol/(m^2 \cdot s \cdot Pa)$]
L = active fiber length, m
N = number of hollow fibers in permeator
p = pressure on permeate side, Pa
P = pressure on feed side, Pa
Q = mass-transfer rate from inner surface of hollow fiber to outer surface, mol/s
R = gas constant, J/(mol·K)
T = temperature, K
U = local molar flow rate of gas in fiber lumen, mol/s
U_0 = molar flow rate of residue product, mol/s
υ = molar average velocity of mass transfer defined by Eq. 14, m/s
V = local molar flow rate of gas in shell side of the permeator, mol/s
X_B = mole fraction of fast gas in the bulk phase
X_0 = mole fraction of fast gas in residue product
X_F = mole fraction of fast gas in feed
X_S = mole fraction of fast gas that the membrane "sees" due to concentration polarization
Y = mole fraction of fast gas in local permeate
Y_P = mole fraction of fast gas in the permeate product
Z = differential active fiber length measured from the residue outlet side, m
δ = thickness of concentration polarization layer, m
θ = stage cut (fraction)

Subscripts

1 = fast gas
2 = slow gas

Literature Cited

Balston Nitrogen Generation Systems, Bulletin PK-62F, Whatman Inc., Haverhill, MA (1997).

Beaver, E. R., P. V. Bhat, and D. S. Sarcia, "Integration of Membranes with Other Air Separation Technologies," *AIChE Symp. Series 261*, Vol. 84, 113 (1988).

Bhide, B. D., and S. A. Stern, "A New Evaluation of Membrane Processes for the Oxygen-Enrichment of Air: I. Identification of Optimum Operating Conditions and Process Configurations," *J. Membrane Sci.*, **62**, 13 (1991a).

Bhide, B. D., and S. A. Stern, "A New Evaluation of Membrane Processes for the Oxygen-Enrichment of Air: II. Effects of Economic Parameters and Membrane," *J. Membrane Sci.*, **62**, 37 (1991b).
Campbell, M. J., R. Prasad, and J. Smolarek, "Membrane/PSA-Deoxo Process for Nitrogen Production," U.S. Patent No. 5,318,759 (1992).
Caskey, T. L., J. L. Jorgensen, and J. L. Trimmer, "Hollow Fiber Membrane Fluid Separation Device Adapted for Boreside Feed," U.S. Patent No. 4,961,760 (1990a).
Caskey, T. L., J. L. Trimmer, and J. L. Jorgensen, "Hollow Fiber Membrane Fluid Separation Module for Boreside Feed," U.S. Patent No. 4,929,259 (1990b).
Crull, A., "Applications for Membrane Technology," presented at the 1998 Sixteenth Annual Membrane Technology/Separations Planning Conference, sponsored by Business Communications Co., Inc., Norwalk, CT (Dec. 7–9, 1998).
Etienne, B. J., W. L. Mills, B. Leprince-Ringuet, and F. Fillet, "Hollow Fiber Membrane Separation Device with a Housing Made from a Flexible Material," U.S. Patent No. 5,380,433 (1995).
Feng, X., and R. Y. M. Huang, "Concentration Polarization in Pervaporation Separation Processes," *J. Membrane Sci.*, **92**, 201 (1994).
Field, R. W., "Mass Transport and the Design of Membrane Systems," *Industrial Membrane Separation Technology*, K. Scott and R. Hughes, eds., Chapman and Hall, p. 67, London, U.K. (1996).
Kalthod, D. G., "Production of Enriched Oxygen Gas Stream Utilizing Hollow Fiber Membranes," U.S. Patent No. 5,500,036 (1996).
Lagree, D. A., and D. R. Thompson, "Duel Product Pressure Swing Adsorption and Membrane Operations," U.S. Patent No. 5,207,806 (1993).
NitroGEN Membrane Nitrogen Supply System, Product Brochure, Praxair Technology Inc., Danbury, CT (1993).
Pan, C. Y., "Gas Separation by Permeators with High-Flux Asymmetric Membranes," *AIChE J.*, **29**, 545 (1983).
Pan, C. Y., "Gas Separation by High-Flux Asymmetric Hollow Fiber Membranes," *AIChE J.*, **32**, 2020 (1986).
Prasad, R., F. Nortara, and D. R. Thompson, "Evolution of Membranes in Commercial Air Separation," *J. Membrane Sci.*, **94**, 225 (1994).
Prism Membrane Nitrogen Systems, Publication No. 522-9601, Air Products and Chemicals Inc., Allentown, PA (1995).
Schaub, H. R., "Membrane/Deoxo Control Method and System," U.S. Patent No. 5,077,029 (1991).
"UBE Nitrogen Gas Generator," Product Brochure, UBE Industries Ltd., Tokyo, Japan (1997).

Manuscript received Apr. 19, 1999, and revision received July 16, 1999.